micro

MDPI

Article

Multi-Response Optimisation of Process Parameter in Abrasive Water Jet Machining of Machining AA7175/ZrB_2 Using Central Composite Design

Jain A. R. Tony Benedict [1], Suthan Ramakrishna Pillai [2,*], Aishwarya Kumaraswamy Pushpa Kumari [3], John Solomon Israel [4], Mohan Raj Manoharan [5], Ayyanar Subbiah [6] and Rajesh Munusamy [7]

1 College of Engineering, Department of Mechanical Engineering, Gulf University, Sanad 26489, Bahrain; dr.jain.tony@gulfuniversity.edu.bh
2 Department of Mechanical Engineering, SRM Institute of Science and Technology, Ramapuram Campus, Ramapuram, Chennai 600089, India
3 Department of Artificial Intelligence and Data Science, Sri Sai Ram Engineering College, West Tambaram, Chennai 600045, India
4 Department of Mechanical Engineering, Panimalar Engineering College, Chennai 600123, India
5 Department of Mechanical Engineering, Karpaga Vinyaga College of Engineering and Technology, Chengalpattu 603308, India
6 Department of Mechanical Engineering, Saveetha School of Engineering, Saveetha Institute of Medical and Technical Science, Chennai 600077, India
7 Department of Mechanical Engineering, Murugappa Polytechnic College, Chennai 600062, India; mvrajesh1991@gmail.com
* Correspondence: itsmesuthan@gmail.com

Abstract

This study examines the impacts of key abrasive water jet machining (AWJM) parameters on the machinability of AA7175–15 wt.% ZrB_2 metal matrix composites produced via a two-step stir casting route. Jet pressure (100–300 MPa), traverse speed (70–130 mm/min), standoff distance (3–5 mm), and abrasive flow rate (250–450 g/min) were systematically varied to evaluate their effects on surface roughness (Ra), kerf taper angle (KA), and material removal rate (MRR). The experimental setup was designed using response surface methodology based on a central composite design (RSM–CCD), enabling both interaction and curvature effects to be assessed. Analysis of variance indicates that jet pressure exerts the strongest influence on MRR, which may be attributed to the increased kinetic energy and penetration capability of abrasive particles at higher pressures. In contrast, traverse speed was found to play a dominant role in controlling surface roughness and kerf geometry. As traverse speed increased, Ra and kerf taper angle tended to rise, likely due to reduced jet–material interaction time and incomplete erosion of the hard ZrB_2-reinforced matrix. Abrasive flow rate contributed positively to MRR up to higher levels, although its effect appeared secondary compared to jet pressure. Regression models developed for all machining responses showed strong predictive performance, with coefficients of determination exceeding 0.95 and statistically insignificant lack-of-fit, suggesting adequate representation of the underlying process behaviour within the investigated parameter range. Scanning electron microscopy of the machined surfaces revealed erosion features such as abrasive ploughing, particle pull-out, and striation formation. These surface morphologies are consistent with the observed variations in Ra and kerf characteristics and reflect the combined ductile–brittle erosion response of the composite. Overall, the study identifies optimised AWJM parameter combinations that can improve both surface quality and machining efficiency when processing AA7175–ZrB_2 composites.

Check for updates

Academic Editor: Sandeep Jain

Received: 7 May 2026
Revised: 30 May 2026
Accepted: 8 June 2026
Published: 21 July 2026

Copyright: © 2026 by the authors. Licensee MDPI, Basel, Switzerland. This article is an open access article distributed under the terms and conditions of the Creative Commons Attribution (CC BY) license.

Keywords: abrasive water jet machining; AA7175; ZrB_2; metal matrix composite; surface roughness; kerf taper

1. Introduction

Aluminium-based metal matrix composites (MMCs) continue to attract sustained interest for aerospace and structural applications, largely because they combine low density with relatively high specific strength and improved wear resistance when compared with monolithic aluminium alloys [1–3]. Within this broader class, high-strength 7xxx-series alloys are often selected for load-bearing components, as their strength-to-weight ratio remains difficult to match using other aluminium systems [4,5]. Also, hard ceramic reinforcements are introduced to further enhance stiffness and hardness, but the benefits come with a clear trade-off: conventional machining becomes increasingly problematic [6,7].

This difficulty is particularly evident in particulate-reinforced aluminium MMCs containing ultra-hard ceramic phases such as zirconium diboride (ZrB_2). ZrB_2 is characterised by high hardness, a high melting point, and good chemical compatibility with aluminium matrices, which together promote grain refinement and effective load transfer during service [8,9]. These attributes also impart improved thermal stability and resistance to high-temperature degradation. From a manufacturing perspective, however, the same properties significantly accelerate tool wear and promote surface damage during conventional cutting operations. Tool–particle interactions tend to be dominated by abrasion and microchipping, which limits achievable surface quality and often leads to premature tool failure. In practice, this constraint necessitates the use of non-traditional machining routes [10].

Abrasive water jet machining (AWJM) has therefore emerged as a viable alternative for machining aluminium MMCs, largely because it is a cold process with negligible heat-affected zones and relatively low cutting forces [11,12]. Material removal in AWJM occurs primarily through high-velocity abrasive particle impacts, involving a combination of micro-cutting, ploughing, and brittle fracture, depending on both process conditions and material response. For aluminium MMCs, this erosion-dominated mechanism avoids many of the tool-related issues encountered in conventional machining [13]. Nevertheless, AWJM performance is far from trivial and depends sensitively on several interacting process parameters.

Previous investigations consistently identify jet pressure, traverse speed, standoff distance, and abrasive flow rate as the primary variables governing AWJM performance [13,14]. Jet pressure is widely regarded as the dominant factor controlling material removal rate (MRR), as it directly influences abrasive particle velocity and, consequently, impact energy. Higher jet pressures generally promote more effective micro-cutting and fracture of hard reinforcements, although the extent of this benefit depends on reinforcement hardness and fracture toughness. Traverse speed plays a different role. By regulating jet–material interaction time, it strongly affects surface roughness and kerf geometry. At higher traverse speeds, the reduced exposure time often results in incomplete erosion at greater depths, which manifests as increased surface roughness and kerf taper, particularly in particle-reinforced systems [15].

Standoff distance further complicates this interaction. At small standoff distances, the jet remains relatively coherent, preserving energy density at the workpiece surface and enabling deeper, more uniform penetration. As standoff distance increases, jet divergence and energy dissipation become more pronounced, leading to reduced cutting efficiency and wider kerf taper [16]. Abrasive flow rate influences the number of effective cutting particles delivered to the surface; however, several studies report diminishing returns beyond an

optimum level. In such cases, particle–particle collisions within the jet reduce individual particle velocity, limiting further gains in erosion efficiency. It is worth noting that the precise balance between these effects remains material dependent [17].

From a materials standpoint, most AWJM studies on aluminium MMCs have focused on AA6061- or AA7075-based composites reinforced with SiC, B_4C, Al_2O_3, or hybrid ceramic particulates. These works provide useful insight into parameter significance and erosion mechanisms, yet their findings cannot be directly extrapolated to diboride-reinforced systems. ZrB_2 differs fundamentally from SiC or B_4C in terms of hardness, elastic modulus, and fracture resistance. As a result, ZrB_2-reinforced aluminium composites require higher impact energy to initiate particle fracture and removal, which alters the prevailing erosion regime during AWJM. Limited studies addressing diboride-reinforced composites suggest increased resistance to erosion, heightened sensitivity to jet pressure, and more pronounced kerf taper under unfavourable conditions [9,11]. However, these studies typically emphasise single-response outcomes or simple parameter ranking, offering limited insight into interaction effects or process non-linearity.

Methodologically, this limitation is compounded by the frequent use of Taguchi-based designs or one-factor-at-a-time approaches, which are inherently inadequate for capturing the coupled and non-linear nature of AWJM processes. The CCD provides a more rigorous framework. It allows regression-based modelling, quantification of interaction and quadratic effects, and simultaneous optimisation of multiple machining responses [18]. Despite these advantages, systematic RSM-based investigations on AWJM of high-strength aluminium MMCs reinforced with ZrB_2 remain scarce. Against this backdrop, systematic multi-response machinability studies on AA7175–ZrB_2 composites are still lacking, especially those that integrate statistical modelling with physically grounded interpretation of erosion mechanisms.

The present study used Central Composite Design (CCD) because of its effectiveness in developing second-order regression models and analysing interaction effects among various parameters in abrasive water jet machining. In contrast to the Taguchi method, which primarily emphasises factor optimisation with restricted interaction analysis, the CCD allows accurate predictions of non-linear interactions and curvature effects among process parameters. In comparison to Box–Behnken Design (BBD), CCD has a more extensive experimental domain due to the inclusion of axial points, hence enhancing the dependability of response surface modelling and optimisation. Moreover, CCD has been widely used in machining research due to its ability to generate precise mathematical models with a reduced number of experimental trials and excellent predictive accuracy for machining reactions, including surface roughness, kerf width, and material removal rate [19,20].

Further, 15 wt.% ZrB_2 was selected to improve the mechanical strength and processability, while keeping the material integrity and processability. A rigorous literature review and early trial tests were carried out before completing this composition to guarantee the uniform distribution of reinforcement and stable machining properties. The selected combination presented an enhanced level of performance compared to lower reinforcement percentages reported in earlier studies [21]. Further, the fabricated composite is subjected to SEM and XRD analysis.

2. Materials and Methods

2.1. AA7175 Base Material

AA7175 aluminium alloy was selected as the matrix material due to its high strength-to-weight ratio and widespread use in load-bearing aerospace and structural components. The alloy was procured commercially from Arihant Aluminium Agencies, Chennai, India, in billet form. Before composite fabrication, the base alloy was characterised to verify its

microstructural integrity and phase constitution. Scanning electron microscopy (SEM) examination revealed a relatively uniform microstructure without observable casting defects such as porosity or microcracks, as shown in Figure 1a. X-ray diffraction (XRD) analysis further confirmed the expected phase composition of AA7175, with no evidence of secondary or impurity phases (Figure 1b). These observations indicate that the base material was suitable for composite processing and subsequent machining studies.

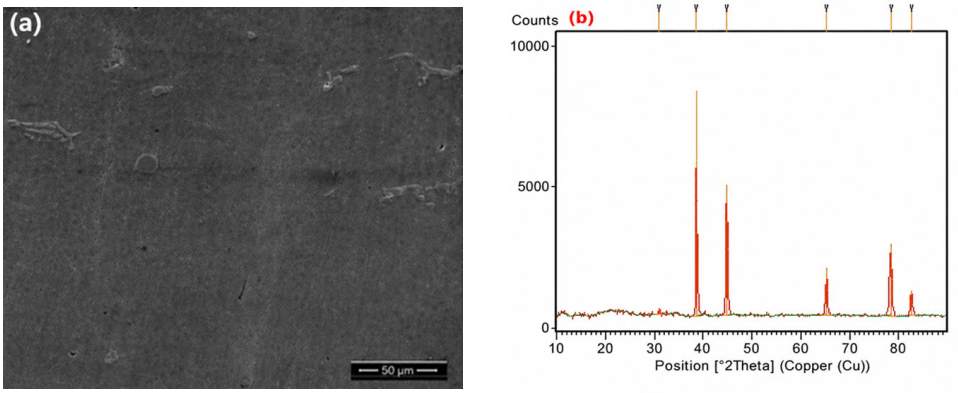


Figure 1. Microstructural examination of AA7175: (**a**) SEM image; (**b**) XRD pattern.

2.2. Zirconium Diboride (ZrB_2) Reinforcement Particles

Zirconium diboride (ZrB_2) particles were used as the ceramic reinforcement owing to their high hardness, thermal stability, and good interfacial compatibility with aluminium matrices. The ZrB_2 powder was procured from M/s. Dalis Electronics Ltd., Mumbai, India. Morphological and phase analyses of the reinforcement were carried out prior to composite fabrication. High-resolution SEM images (Figure 2a) revealed that the ZrB_2 particles exhibit predominantly acicular morphology with a mean particle size of approximately 5.8 µm. The corresponding XRD pattern (Figure 2b) confirmed the presence of phase-pure ZrB_2 without detectable oxide or secondary phases.

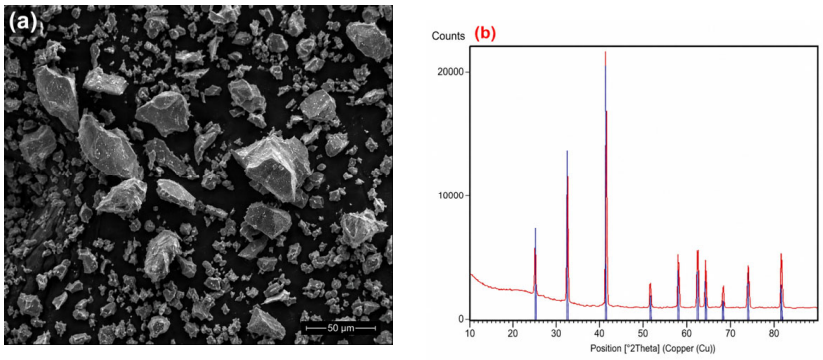


Figure 2. Microstructural examination of ZrB_2 particles: (**a**) SEM image; (**b**) XRD pattern.

2.3. Fabrication of AA7175–15 wt.% ZrB_2 Composite

The AA7175–15 wt.% ZrB_2 composite was fabricated using a two-step stir casting process, selected for its simplicity and scalability in producing particulate-reinforced aluminium composites. Approximately 2 kg of AA7175 alloy was charged into a graphite crucible and melted in an electric resistance furnace. The melting temperature was maintained at 850 ± 1 °C. To minimise moisture-related defects and improve wettability, ZrB_2 particles were preheated separately at 250 °C for 1 h prior to their introduction into the melt. After complete melting of the aluminium alloy, surface dross was carefully removed. A small amount of magnesium (1 wt.%) was then added to the molten alloy to enhance the wetting behaviour between the aluminium matrix and ceramic particles.

Mechanical stirring was carried out using zirconium-coated steel blades to avoid iron contamination. The stirrer was positioned at a distance approximately equal to its radius from the bottom of the crucible, and the stirring speed was maintained at 350 rpm. Once a stable vortex was formed, the preheated ZrB_2 particles were gradually introduced along the periphery of the vortex. Stirring was continued for an additional 2–3 min after particle addition to promote uniform dispersion. The molten composite slurry was finally poured into a preheated metallic die with dimensions of 100 × 100 × 10 mm to obtain flat composite plates suitable for machining experiments. A representative fabricated composite specimen is shown in Figure 3.



Figure 3. Fabricated AA7175–15 wt.% ZrB_2 composite.

2.4. Abrasive Water Jet Machining (AWJM) Experiments

Abrasive water jet machining experiments were conducted to evaluate the machinability of the fabricated AA7175–15 wt.% ZrB_2 composite. Machining trials were performed on an injection-type AWJM system, as illustrated in Figure 4. Garnet abrasive particles with a mesh size of 80 were used throughout the study, and the jet impact angle was maintained at 90° to ensure normal erosion conditions. The thickness of all composite specimens was fixed at 10 mm.



Figure 4. Abrasive water jet machining setup.

A detailed description of the AWJM system specifications and operating conditions is provided in Table 1. The experiments were designed using response surface methodology based on a central composite design (CCD) to capture linear, interaction, and quadratic effects of the process parameters. Four machining parameters were selected as input variables: jet pressure (P), traverse speed (TS), standoff distance (SOD), and abrasive flow rate (AFR). Each parameter was varied over five levels within practical machining limits.

The ranges of parameters chosen for jet pressure, traverse speed, standoff distance (SoD), and abrasive flow rate prior to the test were determined by the results of prior

studies, the limitations of machine operation, and preliminary machining experiments. The jet pressure range was selected to be 100–300 MPa. Minimal pressures were ineffective for efficient cutting, but excessive pressures might lead to significant erosion and unpredictable jet behaviour. The traverse speed range of 70–130 mm/min offers an optimal balance between material removal and surface quality. The standoff distance was selected at 3–5 mm to ensure jet stability and minimise kerf variations during machining. An abrasive flow rate of 250–450 g/min was used to ensure optimal contact with abrasive particles while preventing excessive accumulation of abrasives [22,23]. Figure 5 shows the sample during machining and fabricated sample.

Table 1. Specifications of the abrasive water jet machining system.

Item	Description
AWJM	Injection type nozzle
Power	22 Kw, 50 HZ
Maximum discharge pressure	3200 psi
Abrasive feeding method	Vibratory conveyor
Abrasive particle	Garnet
Shape of abrasive	Random
Mesh Size	80
Jet Impact angle (°)	90
Sample Thickness	10 mm



Figure 5. AA7175–ZrB_2 composite specimens during and after AWJM.

The experimental design matrix and corresponding measured responses are presented in Table 2. A total of 18 experimental runs were conducted, including centre-point repetitions to estimate experimental error and assess model adequacy. The order of experiments was randomised to reduce systematic bias. The output responses considered in this study were surface roughness (Ra), kerf taper angle (KA), and material removal rate (MRR).

Surface roughness measurements were performed using a Taylor Hobson Surtronic contact-type profilometer with a cut-off length of 0.8 mm and an evaluation length of 4 mm. Measurements were taken along the traverse direction, and the reported Ra values represent the average of three repeated measurements for each specimen. Kerf taper angle was determined using top and bottom kerf width measurements obtained from a video measuring system with an accuracy of 0.01 mm, along with the known specimen thickness. The kerf taper angle was calculated using the standard geometric relation. Surface morphology and erosion characteristics of the machined surfaces were examined using a scanning electron microscope.

Table 2. Experimental design matrix and measured responses.

Std	Run	Factor 1, Pressure	Factor 2 SOD	Factor 3 TS	Factor 4 AFR	MRR	SR	KA
15	1	300	3	130	450	5.58	3.689	0.337
16	2	300	5	130	250	5.735	4.192	0.606
8	3	200	4.5	100	350	5.005	4.815	0.78
5	4	200	4	100	300	4.675	4.934	0.821
13	5	150	4	100	350	4.26	5.195	0.924
1	6	200	4	115	350	4.89	4.825	0.804
14	7	100	3	130	250	3.66	5.805	1.27
2	8	300	3	70	450	5.29	3.492	0.182
6	9	200	4	100	350	4.78	4.755	0.761
7	10	250	4	100	350	5.235	4.284	0.58
4	11	200	4	100	400	4.895	4.545	0.698
11	12	200	4	85	350	4.695	4.683	0.711
3	13	200	4.5	100	300	4.879	4.785	0.765
12	14	200	3.5	100	350	4.128	4.705	0.745
17	15	100	3	70	250	2.965	5.646	1.12
9	16	300	5	70	250	5.436	4.025	0.404
10	17	100	5	130	450	3.485	5.475	1.09
18	18	100	5	70	450	4.01	5.302	0.915

3. Results and Discussion

3.1. Microstructure and Phase Analysis of the Composite

The microstructural characteristics and phase constitution of the fabricated AA7175–15 wt.% ZrB_2 composite were examined using SEM and XRD, as shown in Figures 6a and 6b, respectively. SEM observations reveal that ZrB_2 particles are reasonably well distributed within the AA7175 aluminium matrix, with no evidence of large-scale particle agglomeration or macroscopic segregation. While minor local clustering cannot be entirely ruled out an inherent limitation of stir casting the overall dispersion appears sufficiently uniform for subsequent machinability investigations.

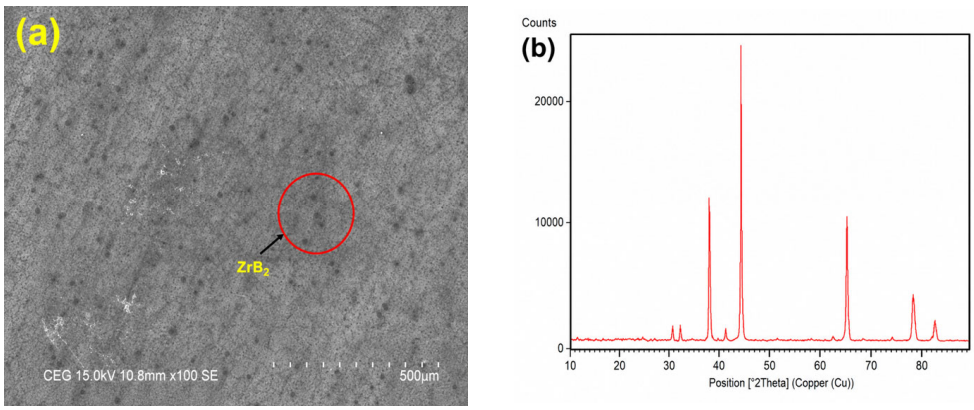


Figure 6. Microstructural and phase analysis: (**a**) SEM image of AA7175/15 wt.% ZrB_2, (**b**) XRD.

A noticeable refinement of the aluminium matrix grains is evident in the composite microstructure. This grain refinement is likely associated with the presence of ZrB_2 particles acting as heterogeneous nucleation sites during solidification, thereby restricting grain growth of the aluminium matrix. Similar grain-refining effects have been reported for diboride-reinforced aluminium systems and are generally attributed to the high thermal stability and crystallographic compatibility of ZrB_2 with aluminium alloys [19]. Such microstructural refinement is expected to contribute to enhanced mechanical performance, although it may also increase resistance to material removal during machining.

The absence of visible oxide layers at the particle–matrix interfaces suggests that the adopted fabrication route, including particle preheating and magnesium addition, was effective in limiting oxidation during processing [24]. In this context, ZrB_2 particles formed or retained within the melt without significant surface oxidation are known to exhibit improved interfacial bonding with aluminium matrices. This improved interfacial condition can reduce the effective wetting angle between the molten aluminium and the ceramic particles, thereby facilitating better particle incorporation and load transfer [25]. However, it should be noted that interfacial quality at the microscale may still vary locally, which can influence erosion behaviour during abrasive water jet machining.

The XRD pattern of the composite, presented in Figure 6b, confirms the presence of ZrB_2 reinforcement within the AA7175 matrix. Distinct diffraction peaks corresponding to ZrB_2 are observed alongside the characteristic aluminium peaks, with no detectable secondary phases or reaction products [26]. The XRD patterns revealed any undesirable secondary phases or brittle intermetallic compounds, indicating the chemical stability of ZrB_2 inside the aluminium matrix.

3.2. Effect of AWJM Process Parameters on Material Removal Rate (MRR)

Material removal rate (MRR) is a practical indicator of machining efficiency in abrasive water jet machining (AWJM). MRR reflects that the influence of the kinetic energy carried by abrasive particles is transferred to the workpiece surface, while accounting for jet stability and the local interaction time. In the present study, the combined effects of jet pressure (P), standoff distance (SOD), traverse speed (TS), and abrasive flow rate (AFR) on the MRR of AA7175–15 wt.% ZrB_2 composites were analysed using a regression-based statistical framework. The ANOVA results are summarised in Table 3, and the corresponding model adequacy metrics are reported in Table 4.

Table 3. ANOVA on material removal rate.

Source	DOF	Sum of Squares	Mean Square	F-Value	*p*-Value
Pressure (P)	1	8.318	8.318	113.87	<0.0001
SOD	1	0.348	0.348	4.76	0.048
Traverse Speed (TS)	1	0.086	0.086	1.18	0.297
Abrasive Flow Rate (AFR)	1	0.042	0.042	0.58	0.46
Residual Error	13	0.950	0.073	—	—
Total	17	9.744	—	—	—

Table 4. Fit statistics.

Metric	Value
R^2	0.9025
Adjusted R^2	0.8725
Model F-value	30.08
Model *p*-value	1.84×10^{-6}
RMSE	0.27
Residual variance (σ^2)	0.073
Durbin–Watson statistic	1.45

The regression model describing MRR was statistically robust, as evidenced by a high model F-value of 113.87 and an associated probability value of less than 0.0001.

Such a low *p*-value strongly suggests that the observed trends are not due to random variation within the experimental window. The coefficient of determination (R^2 = 0.9025) indicates that nearly 98% of the total variability in MRR is captured by the selected AWJM parameters. Importantly, the adjusted R^2 value (0.8725) remained close to R^2, implying that the model retains predictive relevance without artificial inflation due to excessive terms. This point matters, particularly for regression-based optimisation studies, where overfitting can mask physically meaningful trends. The relatively low RMSE (0.27) further supports the adequacy of the model for describing MRR within the investigated parameter space, although extrapolation beyond this range should be approached cautiously.

Among all factors, jet pressure clearly dominated the MRR response, exhibiting the highest F-value. This outcome is physically intuitive and aligns well with established erosion theory. Increasing jet pressure directly increases abrasive particle velocity, and hence the kinetic energy available for material removal scales approximately with the square of velocity. In the case of AA7175–ZrB_2 composites, this additional energy is expended in two parallel mechanisms: plastic deformation and micro-cutting of the aluminium matrix, and brittle fracture or debonding of the ZrB_2 reinforcement. Given the high hardness and elastic modulus of ZrB_2, a threshold impact energy is required to initiate cracking or interfacial failure. Once this threshold is exceeded, reinforcement fragmentation and pull-out become more frequent, contributing disproportionately to mass loss. Similar pressure-dominated behaviour has been reported for particle-reinforced aluminium systems by Ref. [27], although the absolute MRR values reported in the present work are slightly lower, likely due to the relatively high-volume fraction and fracture resistance of ZrB_2.

Standoff distance also exerted a statistically significant, though secondary, influence on MRR. At smaller SOD values, the jet impinges on the surface with higher coherence and energy density, resulting in concentrated impact stresses and efficient erosion (as illustrated in Figure 3). As SOD increases, jet spreading and air entrainment reduce the effective particle velocity at the target surface. This energy loss becomes particularly detrimental when machining hard ceramic reinforcements, where insufficient impact energy may lead to partial matrix erosion without effective particle fracture. While this trend broadly agrees with observations by Mohamed et al. [17] for SiC-reinforced aluminium, the sensitivity of MRR to SOD in the present study appears slightly higher. This may be attributed to differences in particle morphology and interfacial bonding strength between ZrB_2 and the aluminium matrix, although direct microstructural evidence would be needed to confirm this assumption.

Traverse speed showed a clear inverse relationship with MRR, consistent with an erosion-dominated removal mechanism. At lower TS, the jet dwells longer at a given location, allowing repeated abrasive impacts and progressive damage accumulation. This extended interaction time promotes crack initiation within ZrB_2 particles, followed by crack growth, fragmentation, and eventual pull-out. In contrast, at higher traverse speeds, the reduced exposure time limits the number of effective particle impacts per unit area. As a result, erosion becomes incomplete, particularly in regions with a high local reinforcement concentration. This behaviour has been widely reported for metal matrix composites under AWJM, although the degree of MRR reduction with increasing TS can vary depending on reinforcement size and distribution [28].

Compared to the other parameters, abrasive flow rate contributed the least to MRR variation, although its effect remained statistically significant. Increasing AFR increases the population of abrasive particles within the jet, which initially enhances erosion by increasing the frequency of impacts. However, beyond a certain level, intensified particle–particle interactions within the jet can reduce the velocity and impact efficiency of individual abrasives. For hard particle-reinforced composites such as AA7175–ZrB_2, this reduction in

particle velocity is particularly critical, as subcritical impacts may be insufficient to fracture the reinforcement. Consequently, the incremental gain in MRR with increasing AFR diminishes, and AFR assumes a supporting rather than controlling role. Similar saturation-type behaviour has been observed although the onset of saturation in the present study occurs at slightly lower AFR values, possibly due to higher jet loading conditions [29].

Taken together, the statistical trends and mechanistic interpretations consistently indicate that effective energy delivery and retention at the workpiece surface govern MRR during AWJM of AA7175–15 wt.% ZrB_2 composites. Jet pressure primarily controls the available impact energy, while SOD and traverse speed regulate how efficiently that energy is transferred and utilised at the surface. Abrasive flow rate, although necessary to sustain erosion, does not compensate for insufficient particle velocity. From a process optimisation perspective, these findings suggest that maximising MRR requires prioritising pressure and jet coherence, while carefully balancing TS and AFR to avoid inefficient erosion or excessive abrasive consumption. Nevertheless, some uncertainty remains regarding the relative contribution of reinforcement pull-out versus fragmentation, which could be clarified through post-machining microstructural analysis of eroded surfaces.

3.3. Effect of AWJM Process Parameters on Surface Roughness

Surface roughness (Ra) is widely regarded as a critical descriptor of surface integrity in abrasive water jet machining (AWJM), particularly when machining particle-reinforced metal matrix composites. In such systems, material removal does not proceed uniformly. Instead, it evolves through a combination of ductile deformation of the aluminium matrix and brittle fracture or pull-out of ceramic reinforcements. For AA7175–15 wt.% ZrB_2 composites, the pronounced contrast in hardness, stiffness, and fracture behaviour between the matrix and reinforcement introduces competing erosion mechanisms, including micro-cutting, ploughing, interfacial debonding, and particle fragmentation. As a result, the final surface morphology is highly sensitive to process parameters that regulate abrasive particle energy, jet coherence, and the effective interaction time between the jet and the workpiece.

The ANOVA results for surface roughness, along with the associated fit statistics, are presented in Tables 5 and 6. The developed regression model exhibited a high coefficient of determination, indicating that the selected AWJM parameters capture the majority of Ra variation within the explored experimental window. Jet pressure emerged as the most statistically dominant factor influencing surface roughness, followed by abrasive flow rate, traverse speed, and standoff distance. This hierarchy is revealing. It suggests that surface quality in AWJM of ZrB_2-reinforced aluminium composites is governed primarily by parameters that control abrasive particle kinetic energy and impact stability, rather than by kinematic effects alone.

Jet pressure showed a pronounced inverse relationship with surface roughness. At elevated pressures, abrasive particles achieve higher velocities and more consistent trajectories, enabling sustained micro-cutting of the aluminium matrix while simultaneously promoting controlled fracture of ZrB_2 particles. Under these conditions, erosion proceeds in a relatively stable manner, and the tendency for large-scale reinforcement pull-out is reduced. This stabilisation suppresses random ploughing events and limits the formation of deep grooves, resulting in smoother and more uniform surface profiles. In contrast, at lower jet pressures, the impact energy of individual particles may be insufficient to fracture hard ZrB_2 reinforcements or to cut the surrounding matrix cleanly. Instead, localised plastic deformation and interfacial debonding become more prevalent, producing uneven erosion and higher Ra values. The strong statistical contribution of pressure therefore reflects its fundamental role in stabilising the erosion regime across the cutting zone [30].

Table 5. ANOVA on surface roughness.

Source	df	Sum of Squares	Mean Square	F-Value	*p*-Value
Pressure	1	6.2445	6.2445	2323.66	<0.0001
SOD	1	0.0176	0.0176	6.55	0.0238
TS	1	0.0692	0.0692	25.75	<0.001
AFR	1	0.4221	0.4221	157.08	<0.0001
Error	13	0.0349	0.00269	—	—
Total	17	6.788	—	—	—

Table 6. Fit statistics.

Statistic	Value
R^2	0.995
Adjusted R^2	0.993
Model F-value	628.72
Model *p*-value	<0.0001
RMSE	0.0441
Residual variance	0.00206
Durbin–Watson	1.43

Abrasive flow rate ranked as the second most influential parameter affecting Ra. Increasing AFR raises the number of abrasive particles available for material removal, which improves erosion continuity and reduces surface waviness, particularly along the kerf walls. In practical terms, sufficient abrasive availability ensures that material removal proceeds through successive, overlapping micro-cutting events rather than sporadic impacts that promote striation formation. That said, the influence of AFR is not strictly monotonic. At excessively high flow rates, particle–particle interactions within the jet intensify, leading to partial velocity attenuation and less efficient cutting by individual abrasives. In the context of hard particle-reinforced composites, this reduction in effective impact energy can limit further improvements in surface finish. We also observed saturation-type behaviour of Ra with AFR for abrasive-laden high-pressure jets [31].

Traverse speed exhibited a statistically significant, though comparatively weaker, influence on surface roughness. Increasing TS reduces the local jet–material interaction time, thereby limiting the number of effective abrasive impacts per unit length. This reduced exposure promotes incomplete material removal, particularly near ZrB_2 particles where the surrounding aluminium matrix may undergo plastic deformation rather than efficient cutting. As a consequence, erosion becomes less uniform, and surface features such as striations and ploughing marks become more pronounced, especially toward the lower regions of the cut. Although traverse speed clearly affects surface morphology through interaction time effects, its lower statistical contribution suggests that energy-controlled parameters dominate Ra evolution under the present machining conditions. Similar trends have been noted, although the sensitivity to TS can vary depending on reinforcement size and distribution [32].

Standoff distance had the weakest statistical influence on surface roughness within the investigated range, yet its mechanistic role should not be overlooked. At smaller SOD values, the abrasive jet remains relatively coherent, preserving high energy density and consistent particle trajectories at the point of impact. As SOD increases, jet divergence and energy dissipation become more pronounced, resulting in a broader distribution of impact

angles and particle velocities. This loss of coherence promotes uneven erosion, increased waviness, and more pronounced striation patterns, thereby increasing Ra.

Overall, the surface roughness behaviour of AA7175–15 wt.% ZrB_2 composites under AWJM appears to be governed predominantly by parameters controlling abrasive particle energy and delivery stability. Jet pressure and abrasive flow rate dictate whether erosion proceeds via stable micro-cutting or devolves into ploughing and reinforcement pull-out, while traverse speed and standoff distance modulate surface morphology through interaction time and jet coherence effects. These statistical trends are consistent with the surface features observed in scanning electron microscopy, including striation bands, abrasive ploughing grooves, fractured ZrB_2 particles, and localised pull-out cavities. Taken together, the combined statistical and microstructural evidence indicates that achieving low surface roughness in AWJM of particle-reinforced aluminium composites requires prioritising energy-dominated parameters, while treating kinematic controls as secondary but still necessary contributors. Some uncertainty remains regarding the relative contribution of particle fracture versus debonding, which warrants further targeted microstructural investigation.

3.4. Effect of AWJM Process Parameters on Kerf Taper Angle (KA)

Kerf taper angle (KA) reflects how effectively an abrasive water jet retains its cutting capability as it penetrates through the thickness of a workpiece. Unlike surface roughness, which is largely governed by near-surface erosion dynamics, kerf taper is controlled by depth-wise energy dissipation and jet stability. This distinction becomes particularly important in particulate-reinforced aluminium matrix composites, where a ductile aluminium matrix is locally interrupted by hard, erosion-resistant ceramic phases. In AA7175–15 wt.% ZrB_2 composites, taper formation therefore arises from the combined effects of jet divergence, progressive loss of abrasive particle momentum, and the heterogeneous resistance imposed by ZrB_2 reinforcements embedded within the matrix. As a result, KA serves as a sensitive indicator of erosion stability along the cutting depth rather than initial cutting efficiency alone.

The ANOVA results for kerf taper angle, together with the corresponding fit statistics, are summarised in Tables 7 and 8. The regression model exhibited high statistical adequacy, indicating that the selected AWJM parameters capture the dominant physical mechanisms governing taper formation within the investigated parameter window. Among the process variables, jet pressure emerged as the most influential factor affecting KA, followed by abrasive flow rate, traverse speed, and standoff distance. This ranking suggests that kerf geometry is primarily controlled by parameters that regulate abrasive particle momentum retention and impact effectiveness as the jet advances toward the exit region of the cut.

Jet pressure exerted the strongest influence on kerf taper angle, which is consistent with its direct control over abrasive particle velocity and momentum. At higher pressure levels, the jet can sustain sufficient erosive capacity beyond the entry zone, allowing effective material removal to continue deeper into the composite. This reduces the difference between the top and bottom kerf widths, resulting in a lower taper angle (as schematically illustrated in Figure 7). In contrast, at lower pressures, particle energy decays rapidly as the jet penetrates the workpiece. This attenuation is especially pronounced when the jet encounters ZrB_2 particles, which resist erosion and promote premature energy loss. Under such conditions, cutting efficiency deteriorates near the bottom of the kerf, producing a narrower exit width and a pronounced taper. The overwhelming statistical dominance of pressure, therefore, highlights that energy availability, rather than kinematic control, is the primary limiting factor for taper minimisation in hard particle-reinforced aluminium composites [32].

Table 7. ANOVA for Kerf angle.

Source	df	Sum of Squares	Mean Square	F-Value	*p*-Value
Pressure	1	1.0858	1.0858	2986.64	<0.0001
SOD	1	0.00127	0.00127	3.48	0.0848
TS	1	0.06244	0.06244	171.74	<0.0001
AFR	1	0.1015	0.1015	279.06	<0.0001
Error	13	0.00473	0.00036	—	—
Total	17	1.2557	—	—	—

Table 8. Fit statistics.

Statistic	Value
R^2	0.9962
Adjusted R^2	0.9951
Model F-value	860.7
Model *p*-value	<0.0001
RMSE	0.0162
Residual variance	0.000278
Number of runs	1.84

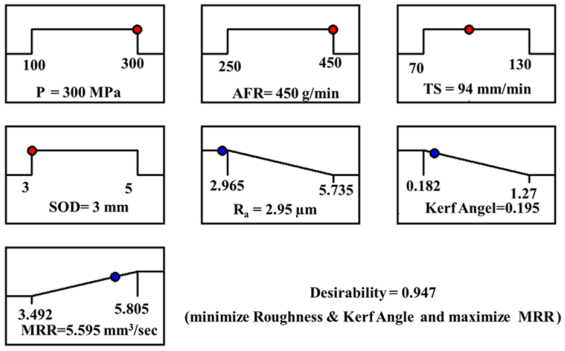


Figure 7. Ramp function graph.

Abrasive flow rate emerged as the second most influential parameter, underscoring the role of abrasive delivery continuity in sustaining cutting effectiveness along the kerf depth. Increasing AFR increases the number of active cutting particles, which helps compensate for the gradual decay in particle energy as the jet progresses through the material. This improved erosion persistence enhances material removal near the bottom of the kerf and reduces taper. That said, the influence of AFR is inherently bounded. At elevated abrasive concentrations, intensified particle–particle interactions within the jet can reduce individual particle velocity and momentum, limiting further gains in kerf geometry. In this sense, AFR improves taper control up to an optimal level, beyond which its effectiveness plateaus.

Traverse speed exhibited a statistically significant but secondary influence on kerf taper formation. Increasing traverse speed reduces the residence time of the jet at any given location, which restricts the extent of material removal in deeper regions of the cut. For ZrB_2-reinforced composites, this reduction in interaction time is particularly detrimental, as sustained jet action is required to erode hard ceramic particles and their surrounding matrix. When exposure time is insufficient, erosion near the bottom of the kerf becomes incomplete, leading to an increased taper angle. Although this mechanism is physically

intuitive, the lower statistical contribution of traverse speed indicates that its effect remains subordinate to that of parameters governing abrasive particle energy.

Standoff distance showed the weakest influence on kerf taper angle within the investigated range. Increasing SOD promotes jet spreading and air entrainment prior to impact, which reduces particle coherence and impact intensity. This degradation in jet quality can marginally impair erosion efficiency at greater depths, thereby contributing to taper formation. However, the relatively low statistical significance of SOD suggests that, under moderate operating conditions, its effect on kerf geometry is limited when compared to pressure and abrasive flow rate. It is likely that SOD would play a more pronounced role outside the present range, particularly at excessively large stand-off distances, although this was not explored here.

Overall, the kerf taper behaviour observed during AWJM of AA7175–15 wt.% ZrB_2 composites indicates that dimensional accuracy is governed primarily by the jet's ability to retain abrasive particle momentum throughout the cutting depth. Parameters that directly control particle energy and abrasive delivery dominate taper formation, whereas kinematic and geometric parameters exert secondary, moderating effects. From a process control perspective, these findings imply that minimising kerf taper in particle-reinforced aluminium composites requires prioritising energy-dominated parameters to ensure stable erosion from entry to exit. Some uncertainty remains regarding the relative contribution of reinforcement fracture versus interfacial debonding near the kerf bottom, which could be clarified through detailed subsurface microstructural analysis.

3.5. Optimisation and Validation

The quality evaluation of the machined composites considers different variables. To determine the optimal levels of the machining variables that affect the multiple responses, the desirability function approach was employed. In this method, the responses are transformed into a dimensionless desirability value (D) using Equation (1). As shown in Table 9, the parameters for the optimisation process were based on minimising kerf angle and Ra and maximising MRR with the maximum significance assigned to the specified machining conditions.

$$= \left(\sum_{i=1}^{n} d_i \right)^{1/n} \quad (1)$$

where d_i is the corresponding response and n is the number of responses;
d_i = 1 when the predicted response value is less than the obtained lower value;
d_i = 0 when the predicted response value is greater than the obtained higher value.

Table 9. Optimisation condition: minimise kerf angle and R_a and maximise MRR.

Input AWJD Variables	Unit	Assigned Target	Limit		Importance	Optimised Values
			Low	High		
P	MPa	is in range	100	300	5	300
SOD	mm	is in range	3	5	5	3
TS	mm/min	is in range	70	130	5	94
AFR	g/min	is in range	250	450	5	450
R_a	µm	minimise	2.965	5.735	5	2.95
Kerf angle	Degree	minimise	0.182	1.27	5	0.195
MRR	mm^3/s	maximise	3.492	5.805	5	5.595

Figure 7 (ramp graph) represents the desirability of the parameters and response. It helps visualise the trade-offs between different parameters and responses, allowing us to identify the combination of parameter settings that leads to the desired overall performance.

Validation

The AWJ experiments were conducted on composite settings that optimised the parameters as shown in Table 10. It was found that the error was less than 5%. The fact that the findings were verified by experimentation with a deviation below 5% indicates that the established optimisation framework is both statistically sound and practically applicable.

Table 10. Validation analysis.

P	AFR	TS	SOD	Predict			Actual			Error%		
				R_a	KA	MRR	R_a	KA	MRR	R_a	KA	MRR
300	450	94	3	2.95	0.195	5.595	2.98	0.199	5.532	1.02	2.05	1.13

3.6. SEM-Based Surface Morphology and Erosion Mechanisms

Scanning electron microscopy (SEM) was employed to examine the surface morphology of AWJM-machined AA7175–15 wt.% ZrB_2 composites to identify the dominant erosion mechanisms and to establish microstructural correlations with the observed machining responses. Representative SEM micrographs are presented in Figure 8.

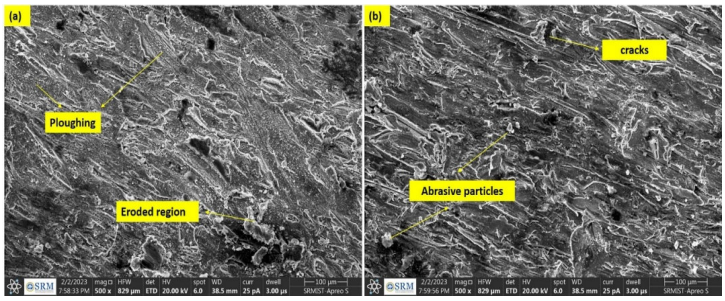


Figure 8. SEM micrographs of AWJM-machined AA7175–15 wt.% ZrB_2 composite surfaces under different machining conditions. (**a**) SEM image of low abrasive flow condition (**b**) SEM image of higher abrasive flow condition.

The SEM observations indicate that material removal during AWJM of the ZrB_2-reinforced composite occurs through a combination of micro-cutting of the aluminium matrix, abrasive ploughing, brittle fracture of ZrB_2 particles, and reinforcement particle pull-out. The relative contribution of these mechanisms varies significantly with machining parameters, reflecting changes in abrasive particle energy, jet coherence, and jet–material interaction time. Under favourable machining conditions, characterised by higher jet pressure and lower traverse speed, the machined surfaces exhibit comparatively smooth topographies with fine, uniformly distributed striations aligned with the jet traversal direction [29].

In these cases, abrasive particles possess sufficient kinetic energy to penetrate the aluminium matrix and induce brittle fracture of ZrB_2 particles rather than their debonding. As a result, erosion proceeds more stably and uniformly, which is consistent with the lower surface roughness and reduced kerf taper observed under these conditions, as evident from Figure 8a. Only limited evidence of particle pull-out is observed, suggesting effective interfacial bonding and efficient energy transfer from the abrasive particles to the composite.

In contrast, surfaces machined at higher traverse speeds show pronounced striation patterns, irregular grooves, and localised surface damage. The reduced jet–material interac-

tion time under these conditions' limits repeated abrasive impacts, leading to incomplete erosion and non-uniform material removal, particularly at greater cutting depths [29].

Figure 8b depicts the partially fractured ZrB_2 particles embedded within smeared aluminium matrix regions, indicating insufficient impact energy for complete particle removal. These features correlate well with the experimentally observed increase in surface roughness and kerf taper angle at higher traverse speeds. An increase in standoff distance further exacerbates erosion instability, as evidenced by widened striation spacing and uneven erosion patterns on the machined surfaces. Greater standoff distances promote jet divergence and air entrainment, resulting in reduced particle velocity and dispersed impact angles at the workpiece surface. This loss of jet coherence diminishes erosive effectiveness at the lower regions of the cut, contributing to higher kerf taper and rougher surface profiles. Under such conditions, particle pull-out becomes more prevalent, likely due to localised stress concentrations at the particle–matrix interface combined with insufficient fracture energy [31].

The influence of abrasive flow rate on surface morphology is comparatively subtle but still discernible. At moderate abrasive flow rates, SEM images show improved erosion uniformity, reflecting a sufficient population of effective cutting particles [26]. However, at higher abrasive flow rates, surface damage becomes more pronounced, with increased ploughing marks and surface irregularities. This behaviour may be attributed to particle crowding and inter-particle collisions within the jet, which reduce individual particle velocity and limit effective penetration. These observations are consistent with the statistically identified secondary role of abrasive flow rate in governing surface roughness and kerf characteristics.

Overall, the SEM-based morphological analysis provides direct physical evidence supporting the trends identified through ANOVA and regression modelling. Improved surface integrity and reduced kerf taper are associated with machining conditions that maintain jet coherence and sufficient abrasive particle energy throughout the cutting depth. Conversely, degraded surface quality and increased taper arise under conditions that promote rapid energy dissipation and unstable erosion. This strong agreement between microstructural observations and statistical analysis reinforces the reliability of the developed models and the proposed machinability trends for AWJM of AA7175–ZrB_2 composites.

4. Conclusions

The present study systematically examined the machinability of AA7175–15 wt.% ZrB_2 metal matrix composites fabricated by a two-step stir casting route using abrasive water jet machining. Response surface methodology based on a central composite design was employed to quantify and optimise the effects of jet pressure, traverse speed, standoff distance, and abrasive flow rate on material removal rate (MRR), surface roughness (Ra), and kerf taper angle (KA). Based on the experimental results, statistical analysis, and microstructural observations, the following conclusions can be drawn:

1. Jet pressure was identified as the dominant parameter governing material removal rate. Higher pressure levels significantly increased MRR by enhancing abrasive particle velocity and impact energy, thereby promoting effective micro-cutting of the aluminium matrix and brittle fracture of embedded ZrB_2 particles.
2. Traverse speed exerted the strongest influence on surface roughness and kerf taper angle. Lower traverse speeds improved surface finish and reduced kerf taper by increasing jet–material interaction time, enabling more uniform erosion and sustained material removal through the composite thickness.
3. Standoff distance played a critical role in maintaining jet coherence and penetration capability. Reduced standoff distances preserved energy density at the workpiece sur-

face, resulting in smoother surfaces and lower kerf taper, whereas excessive standoff distances led to jet divergence, rapid energy dissipation, and non-uniform erosion.

4. Abrasive flow rate exhibited a secondary but statistically significant influence on all machining responses. Moderate abrasive flow rates enhanced erosion uniformity, while excessively high flow rates offered limited additional benefit due to particle–particle interactions that reduced effective particle velocity.
5. The developed RSM-based regression models demonstrated strong predictive capability for all responses, with coefficients of determination exceeding 0.95 and statistically insignificant lack-of-fit, confirming their suitability for process prediction and multi-response optimisation within the investigated parameter range.
6. SEM-based surface morphology analysis revealed erosion mechanisms dominated by abrasive micro-cutting, ploughing, brittle fracture of ZrB_2 particles, and particle pull-out. These mechanisms showed strong correlation with the statistically observed trends in MRR, Ra, and KA, providing physical validation of the developed models.

This study establishes optimised AWJM parameter windows for improving machining efficiency and surface integrity of AA7175–ZrB_2 composites and provides mechanistic insight into erosion-controlled material removal in hard particle-reinforced aluminium alloys. The findings are expected to assist in the effective machining of advanced aluminium MMCs where conventional cutting methods are limited.

Author Contributions: Conceptualization, J.A.R.T.B. and S.R.P.; methodology, J.A.R.T.B.; software, A.K.P.K.; validation, J.A.R.T.B., S.R.P., and J.S.I.; formal analysis, M.R.M.; investigation, J.A.R.T.B.; resources, A.S.; data curation, A.K.P.K.; writing—original draft preparation, J.A.R.T.B.; writing—review and editing, S.R.P., J.S.I., and R.M.; visualization, M.R.M.; supervision, S.R.P.; project administration, J.A.R.T.B., R.M. All authors have read and agreed to the published version of the manuscript.

Funding: This research received no external funding.

Institutional Review Board Statement: Not applicable.

Informed Consent Statement: Not applicable.

Data Availability Statement: The data presented in this study are available on request from the corresponding author.

Conflicts of Interest: The authors declare no conflicts of interest or state.

References

1. Lakshmikanthan, A.; Angadi, S.; Malik, V.; Saxena, K.K.; Prakash, C.; Dixit, S.; Mohammed, K.A. Mechanical and tribological properties of aluminum-based metal-matrix composites. *Materials* **2022**, *15*, 6111. [CrossRef]
2. Gupta, P.K.; Trivedi, A.K.; Gupta, M.K.; Dixit, M. Metal matrix composites for sustainable products: A review on current development. *Proc. Inst. Mech. Eng. Part L J. Mater. Des. Appl.* **2024**, *238*, 1827–1864. [CrossRef]
3. Deshmukh, S.; Joshi, G.; Ingle, A.; Thakur, D. An overview of aluminium matrix composites: Particulate reinforcements, manufacturing, modelling and machining. *Mater. Today Proc.* **2021**, *46*, 8410–8416. [CrossRef]
4. Zhou, B.; Liu, B.; Zhang, S. The advancement of 7xxx series aluminum alloys for aircraft structures: A review. *Metals* **2021**, *11*, 718. [CrossRef]
5. Thavasilingam, K.; Sakthimurugan, D.; Giridharan, K. Aluminum alloys for aircraft structures. In *Aerospace Materials*; Elsevier: Amsterdam, The Netherlands, 2025; pp. 385–404.
6. Varikkadinmel, B.; Inderdeep, S. Role of ceramics in machining of composite materials: A comprehensive review. *Int. J. Appl. Ceram. Technol.* **2025**, *22*, e14999.
7. Fu, L.; Yu, W.; Wang, B.; Lei, Z.; Deng, M.; Liu, G.; Cai, G. Architecting dual heterogeneous structures to achieve robust mechanical properties in ZrO2-SiO2 nanocrystalline ceramics. *J. Am. Ceram. Soc.* **2026**, *109*, e70386.
8. Kumar, V.; Kulkarni, N.M.; Sinha, N.K.; Ji, G.; Katiyar, J.K.; Singh, M.K. Physico-tribomechanical performance of Zn-Al/ZrB2 in-situ composite for sustainable automotive applications. *Tribol. Int.* **2025**, *206*, 110591. [CrossRef]

9. Dinaharan, I.; Murugan, N.; Parameswaran, S. Influence of in situ formed ZrB2 particles on microstructure and mechanical properties of AA6061 metal matrix composites. *Mater. Sci. Eng. A* **2011**, *528*, 5733–5740. [CrossRef]
10. Kumar, P.; Kumar, B. Effect of T6 heat treatment on mechanical and tribological properties of fabricated AA7075/ZrB2/Fly ash hybrid aluminum metal matrix composite by ultrasonic-assisted stir casting enroute. *Int. J. Met.* **2024**, *18*, 2396–2414. [CrossRef]
11. Thamizhvalavan, P.; Varatharajulu, M.; Baskaran, J. Parametric optimization of abrasive waterjet machining for aluminum 7075/boron carbide/zirconium silicate hybrid composites. *Proc. Inst. Mech. Eng. Part E J. Process Mech. Eng.* **2025**, 09544089241312610.
12. Natarajan, Y.; Murugesan, P.K.; Mohan, M.; Khan, S.A.L.A. Abrasive Water Jet Machining process: A state of art of review. *J. Manuf. Process.* **2020**, *49*, 271–322. [CrossRef]
13. Kishawy, H.A.; Hosseini, A. Machining difficult-to-cut materials. *Mater. Form. Mach. Tribol.* **2019**, *10*, 973–978.
14. Mohan, M.; Radhakrishnan, M.; Ganapathy, V.B.; Thirugnanasambandam, A. Coupled Numerical–Experimental Study on Water Jet Peening for Surface Integrity Enhancement of AZ31B Magnesium Alloy in Biomedical Applications. *Mater. Today Commun.* **2025**, *49*, 114287. [CrossRef]
15. Llanto, J.M.; Tolouei-Rad, M.; Vafadar, A.; Aamir, M. Impacts of traverse speed and material thickness on abrasive waterjet contour cutting of austenitic stainless steel AISI 304L. *Appl. Sci.* **2021**, *11*, 4925. [CrossRef]
16. Ibrahim, A. Controlled Depth Micro-Milling of Aluminum Oxide Using Abrasive Waterjet Machining to Create Micro-Molds with Free-Standing structures. Doctoral Dissertation, Toronto Metropolitan University, Toronto, Canada, 2024.
17. Mohamad, W.N.F.; Kasim, M.S.; Norazlina, M.Y.; Hafiz, M.S.A.; Izamshah, R.; Mohamed, S.B. Effect of standoff distance on the kerf characteristic during abrasive water jet machining. *Results Eng.* **2020**, *6*, 100101. [CrossRef]
18. Tolcha, M.A.; Lemu, H.G.; Adugna, Y.W. Optimizing economics of machining for LM25Al/VC composite material using analytical modeling, deep neural network and GRA coupled with RSM. *Sci. Rep.* **2025**, *15*, 10215. [CrossRef] [PubMed]
19. Jensen, W.A. *Response Surface Methodology: Process and Product Optimization Using Designed Experiments*, 4th ed.; Wiley: Hoboken, NJ, USA, 2017.
20. Kilickap, E.; Huseyinoglu, M.; Yardimeden, A. Optimization of drilling parameters on surface roughness in drilling of AISI 1045 using response surface methodology and genetic algorithm. *Int. J. Adv. Manuf. Technol.* **2011**, *52*, 79–88.
21. Loganathan, P.; Gnanavelbabu, A.; Rajkumar, K. Analysis and characterization of friction behaviour on AA7075/ZrB_2 composite under dry sliding condition. *Mater. Res. Express* **2019**, *6*, 026576. [CrossRef]
22. Kumar, K.R.; Sreebalaji, V.S.; Pridhar, T. Characterization and optimization of abrasive water jet machining parameters of aluminium/tungsten carbide composites. *Measurement* **2018**, *117*, 57–66. [CrossRef]
23. Manoj, M.; Jinu, G.R.; Kumar, J.S. Process optimization of abrasive water jet machining of aluminum hybrid composite using Taguchi DEAR methodology. *Int. J. Met.* **2024**, *18*, 933–943.
24. Bañon, F.; Sambruno, A.; Mayuet, P.F.; Gómez-Parra, Á. Study of abrasive water jet machining as a texturing operation for thin aluminium alloy UNS A92024. *Materials* **2023**, *16*, 3843. [CrossRef] [PubMed]
25. El Midany, T.; Ahmed, T.; El Mesalamy, A.S.; Youssef, A.M. Experimental study and modelling of abrasive water jet cutting of aluminum alloy 2024. *J. Eng. Sci. Mil. Technol.* **2019**, *3*, 14–22. [CrossRef]
26. Sathees Kumar, S.; Isaac Premkumar, I.J.; Muthalagu, R.; Vijayakumar, S.; Pradeep, A.; Naga Swapna Sri, M. Examination of Abrasive water jet machining for Al hybrid composites using RSM-Central composite design. *Interactions* **2024**, *245*, 220. [CrossRef]
27. Kartal, F.; Kaptan, A. Artificial neural network and multiple regression analysis for predicting abrasive water jet cutting of Al 7068 aerospace alloy. *Sigma J. Eng. Nat. Sci.* **2024**, *42*, 516–528. [CrossRef]
28. Shanmugam, A.; Krishnamurthy, K.; Mohanraj, T. Experimental study of surface roughness and taper angle in abrasive water jet machining of 7075 aluminum composite using response surface methodology. *Surf. Rev. Lett.* **2020**, *27*, 1950112.
29. Gnanavelbabu, A.; Rajkumar, K.; Saravanan, P. Investigation on the cutting quality characteristics of abrasive water jet machining of AA6061-B4C-hBN hybrid metal matrix composites. *Mater. Manuf. Process.* **2018**, *33*, 1313–1323. [CrossRef]
30. Prakash, C.; Selvakumar, S.; Manikandan, D.; Ramaswamy, K. Machinability analysis of LM26 aluminium metal matrix composites reinforced with graphite and fly Ash using the AWJM process. *Sci. Rep.* **2025**, *15*, 23613. [CrossRef] [PubMed]
31. Mohan, M.; Kaliyamoorthy, R. Integrated TOPSIS and machine learning-based predictive modelling for optimising abrasive water jet drilling of glass–sisal and glass–sisal–jute hybrid polymer laminates. *Int. J. Interact. Des. Manuf. (IJIDeM)* **2026**, *20*, 3547–3569. [CrossRef]
32. Manjunath Patel, G.C.; Jagadish Kumar, R.S.; Naidu, N.S. Optimization of abrasive water jet machining for green composites using multi-variant hybrid techniques. In *Optimization of Manufacturing Processes*; Springer International Publishing: Cham, Switzerland, 2019; pp. 129–162.

Disclaimer/Publisher's Note: The statements, opinions and data contained in all publications are solely those of the individual author(s) and contributor(s) and not of MDPI and/or the editor(s). MDPI and/or the editor(s) disclaim responsibility for any injury to people or property resulting from any ideas, methods, instructions or products referred to in the content.